Available on CMS information server

CMS AN -2009/169

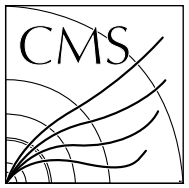

The Compact Muon Solenoid Experiment

Analysis Note

The content of this note is intended for CMS internal use and distribution only

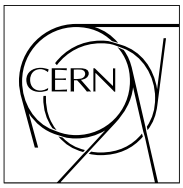

17 November 2009

Towards a Measurement of $pp \to Z(\to \ell^+\ell^-)\gamma$ and Study of Anomalous Trilinear Gauge Coupling Sensitivity with CMS in the Electron and Muon Channels

P. Adzic, S. Dasu, M. Djordjevic, L. Gray, C. Karafasoulis, A. Kyriakis, A. Markou, and E. Petrakou

Abstract

This note describes the preparations towards searching for the production of a Z boson in association with a photon at the LHC with $\sqrt{s} = 10$ TeV in the first 200 pb^{-1} of data. A sensitivity analysis investigating a search for anomalous couplings of the Z and photon is also presented. These studies are performed using both Pythia 6 and a modified event generator from U. Baur to produce signal samples. Background samples used are CMS production monte carlo.

Contents

1 Introduction

1.1 $Z\gamma$ couplings

The couplings between gauge bosons are of particular importance in the Standard Model (SM) since they reflect the very essence of the model, its symmetry structure. As the properties of the couplings are accurately defined by the spontaneously broken, non-Abelian gauge theory of weak interactions, they serve as important tests of the known physics and they are sensitive to new phenomena beyond the SM.

In proton-proton collisions at the LHC the trilinear gauge couplings (TGCs) can be studied via di-boson final states. In the case of triple boson vertices involving the Z boson, only the WWZ vertex is allowed at Born level within the SM, since any neutral couplings are prohibited. Thus, the only leading-order SM Feynman diagrams for the $Z\gamma$ processes are obtained by substituting $V_1 = Z$ and $V_2 = \gamma$ in Fig. 1(a) and 1(b). The anomalous TGCs ("aTGCs") contribution can be obtained from the diagram of Fig. 1(c) by substituting $V_0 = \gamma$ or Z. Observation of aTGCs through $Z\gamma$ production would be direct evidence of new physics.

Current precision electroweak measurements indicate that the SM may only be valid at low energies. The experimental search for the contributions of aTGCs to the production of boson pairs benefits from a parameterization independent of any particular theoretical model. This is possible with the use of an effective Lagrangian which includes all possible terms of three vector bosons, by imposing only the most general restrictions: By requiring Lorentz invariance of the on-shell photon and electromagnetic gauge invariance, and assuming negligible lepton masses, the function of the $Z\gamma V(V = Z, \gamma$ virtual) vertex can be parameterized using eight free parameters [1]:

$$
\begin{aligned}
&Z(q_1)\gamma(q_2)V(P): \\
&\Gamma^{\alpha\beta\mu}_{Z\gamma V}(q_1, q_2, P) = \mathcal{A}^V \cdot [h_1^V (q_2^\mu g^{\alpha\beta} - q_2^\alpha g^{\mu\beta}) + \frac{h_2^V}{m_Z^2} P^\alpha [(P \cdot q_2) g^{\mu\beta} - q_2^\mu P^\beta] \\
&\qquad + h_3^V \epsilon^{\mu\alpha\beta\rho} q_{2\rho} + \frac{h_4^V}{m_Z^2} P^\alpha \epsilon^{\mu\beta\rho\sigma} P_\rho q_{2\sigma}],
\end{aligned}
\tag{1}
$$

where for $V = Z$: $\mathcal{A}^Z = \frac{P^2 - q_1^2}{m_Z^2}$, while for $V = \gamma$: $\mathcal{A}^\gamma = \frac{P^2}{m_Z^2}$

The eight couplings h_i^V are dimensionless functions of the squared momenta. The couplings h_1^V and h_2^V are CP-violating, while h_3^V and h_4^V are CP-conserving. These couplings have no physical meaning, but are related to the electric and magnetic dipole and quadrupole moments of the $V - Z$ transition [2][3]:

$$
\begin{aligned}
d_Z &= -\tfrac{e}{M_Z} \tfrac{1}{\sqrt{2}} \tfrac{k^2}{M_Z^2} (h_3^V - h_4^V) && \text{Electric dipole transition moment} \\
Q_Z^e &= \tfrac{e}{M_Z^2} \sqrt{1}\, (2h_1^V) && \text{Electric quadrupole transition moment} \\
\mu_Z &= -\tfrac{e}{M_Z} \tfrac{1}{\sqrt{2}} \tfrac{k^2}{M_Z^2} (h_1^V - h_2^V) && \text{Magnetic dipole transition moment} \\
Q_Z^\mu &= \tfrac{e}{M_Z^2} \sqrt{10} (2h_3^V) && \text{Magnetic quadrupole transition moment}
\end{aligned}
$$

In the SM all couplings h_i^V vanish at leading order, but at one-loop level the CP-conserving $h_{3,4}^V$ are non-zero [4].

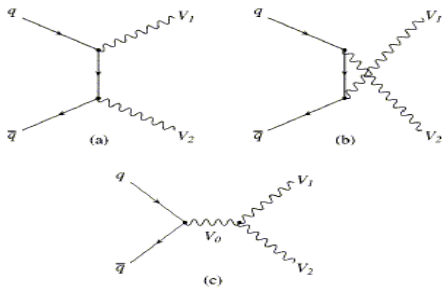

Figure 1: Leading-order SM Feynman diagrams for the vector boson pair production. The $Z\gamma$ processes are obtained by substituting $V_0 = \gamma$ or Z, $V_1 = Z$ and $V_2 = \gamma$.

Baur et al. [5][6] have used helicity amplitude techniques to calculate the contribution of the $Z\gamma V$ diagrams to the $Z\gamma$ production cross-section. They also provided software for cross-section calculation at leading and next-to-leading logarithmic contributions and QCD corrections.

A crucial consideration when studying the aTGCs is partial-wave unitarity. Since the h_i^V couplings depend on the particle momenta, the preservation of unitarity at high centre-of-mass energies must be ensured; this implies that h_i^V's have to be described by form factors which fall off rapidly for large momenta and should vanish asymptotically at high energies, essentially restricting the couplings to their SM values.
The unitarity bounds can first be derived for the helicity amplitudes, and then "translated" to the couplings[5], assuming that the latter are expressed by dipole form factors:

$$h_i^V(q_1 = m_Z^2, q_2 = 0, P = \hat{s}) \;=\; \frac{h_{i0}^V}{(1 + \hat{s}/\Lambda^2)^n},$$

where Λ is the cutoff scale, i.e. the energy at which the novel interactions causing the deviation of h_i^V's from their SM values start to appear. The assumption that only one aTGC is non-zero at a time leads to the following unitarity bounds for $\Lambda >> m_Z$:

$$|h_{10}^Z|, |h_{30}^Z| \;<\; \frac{(\frac{2}{3}n)^n}{(\frac{2}{3}n - 1)^{n-3/2}} \frac{0.126\, TeV^3}{\Lambda^3},$$

$$|h_{20}^Z|, |h_{40}^Z| \;<\; \frac{(\frac{2}{5}n)^n}{(\frac{2}{5}n - 1)^{n-5/2}} \frac{2.1 \times 10^{-3}\, TeV^5}{\Lambda^5},$$

$$|h_{10}^\gamma|, |h_{30}^\gamma| \;<\; \frac{(\frac{2}{3}n)^n}{(\frac{2}{3}n - 1)^{n-3/2}} \frac{0.151\, TeV^3}{\Lambda^3},$$

$$|h_{20}^\gamma|, |h_{40}^\gamma| \;<\; \frac{(\frac{2}{5}n)^n}{(\frac{2}{5}n - 1)^{n-5/2}} \frac{2.5 \times 10^{-3}\, TeV^5}{\Lambda^5}.$$

The exponent n is arbitrary and model-dependent, and has to be provided along with Λ. However, it must be $n > \frac{3}{2}$ for $h_{1,3}^V$ and $n > \frac{5}{2}$ for $h_{2,4}^V$ to preserve unitarity. In the case that more than one couplings are non-zero, the bounds may be weaker due to cancelations.

2 Analysis Using CMS Production Signal Monte Carlo Sample

The following sections detail an analysis of the $Z\gamma$ signal and its backgrounds using a sample of signal events produced in CMSSW 2.2.13 with Pythia 6 and $\sqrt{s}$ = 10 TeV to simulate the hard scatter and underlying event. The backgrounds included are $Z + Jets$, $W + Jets$, $t\bar{t}$, EM and Muon enriched QCD samples. All plots are scaled to an integrated luminosity of 200 pb^{-1}.

2.1 Signal and Background

The matrix element for $f\bar{f} \rightarrow \ell^+\ell^-\gamma$ is calculated by U. Baur [6] and T. Sjöstrand [7]. The implementation in Pythia is different with respect to U. Baur's matrix element generator since it does not include tunable anomalous couplings. Hence, this study is focused on detecting the Standard Model $Z\gamma$ signal and measuring its cross section. Additional optimizations are given for increased acceptance and purity in the high photon E_T region, which is of interest in the anomalous coupling search.

We generate the signal sample using Pythia 6, requiring that the matrix element photon be generated with $E_T > 10$ GeV with a cross section of $3.7pb^{-1}$ per lepton channel. The Z is allowed to decay to electrons, muons or taus. In this study, only the electron and muon decay modes are of interest. Therefore, at least one opposite sign same flavor lepton pair and at least one reconstructed photon are required in the event. Interesting distributions include the photon p_T and diboson invariant mass spectra; these plots are useful both in a standard model $Z\gamma$ analysis and in searches for new physics due to enhancements in the differential cross sections at high diboson mass and high photon E_T.

The primary background to the $Z\gamma$ signal comes from $Z + Jets$ when one of the jets fakes a photon by fragmenting primarily to π^0s. Hadronization of this sort occurs with frequency of 1 in 1000 jets, as measured by the CDF Collaboration [8]. Hence, we should expect the cross section of $Z + Jet$ events where the Z decays to leptons and one of the jets fakes a photon to be roughly 1.2 pb^{-1} [9], making the theoretically predicted signal to background ratio roughly 3 to 1. The $Z + Jets$ background is simulated using MadGraph for the hard scatter and Pythia 6 for hadronization.

The secondary backgrounds to the $Z\gamma$ signal are:

- $t\bar{t} \rightarrow \ell^+\ell^- + X$, ℓ = e, μ, where the photon is real or a misreconstructed jet;
- $p\bar{p} \rightarrow W^{\pm}(\rightarrow \ell^{\pm}\nu_{\ell}) + Jets$, other particles are picked up through misreconstruction or underlying event;
- QCD processes which produce lepton pairs, photons and jets.

These backgrounds are non-peaking and tend to require multiple misreconstructions. Therefore, they are removed using invariant mass cuts on the lepton pair as well as lepton and photon identification.

2.2 Event Selection

To start, we define the preselection for the class of events being studied. In order for the event to be considered it must contain at least one electron or muon passing the "L1IsoLargeWindowSingleElectronTrackIsolFilter" or "SingleMuNoIsoL3PreFiltered" trigger filters, respectively. The di-muon trigger will be included for additional η coverage in future iterations of this analysis. After the triggering requirement, the leptons in the event are combined into opposite sign same flavor pairs, requiring that one of the leptons in each pair be triggered, and further that dilepton mass is within 60 GeV of the Z pole mass. We require the existence of at least one

Table 1: Datasets used in this analysis. [10]

Dataset	σ at 10 TeV	Filter Efficiency
/Zgamma/Summer08_IDEAL_V11_redigi_v1/GEN-SIM-RECO	11 pb	1.0
/ZJets-madgraph/Summer08_IDEAL_V11_redigi_v1/GEN-SIM-RECO	3.7 nb	.40
/WJets-madgraph/Summer08_IDEAL_V11_redigi_v1/GEN-SIM-RECO	40 nb	.45
/TauolaTTbar/Summer08_IDEAL_V11_redigi_v2/GEN-SIM-RECO	241.7 pb	1.0
/QCD_EMenriched_Pt20to30/Summer08_IDEAL_V11_redigi_v2/GEN-SIM-RECO	.40 mb	.0080
/QCD_EMenriched_Pt30to80/Summer08_IDEAL_V11_redigi_v2/GEN-SIM-RECO	.10 mb	.047
/InclusiveMuPt15/Summer08_IDEAL_V11_redigi_v1/GEN-SIM-RECO	.5091 mb	.000239

such pair. Next we require the presence of a reconstructed photon within the tracking volume with $E_T > 25$ GeV and $H/E < .2$. If these criteria are met the event is considered for further analysis. The resulting dilepton invariant mass distribution is shown in Figure 2.

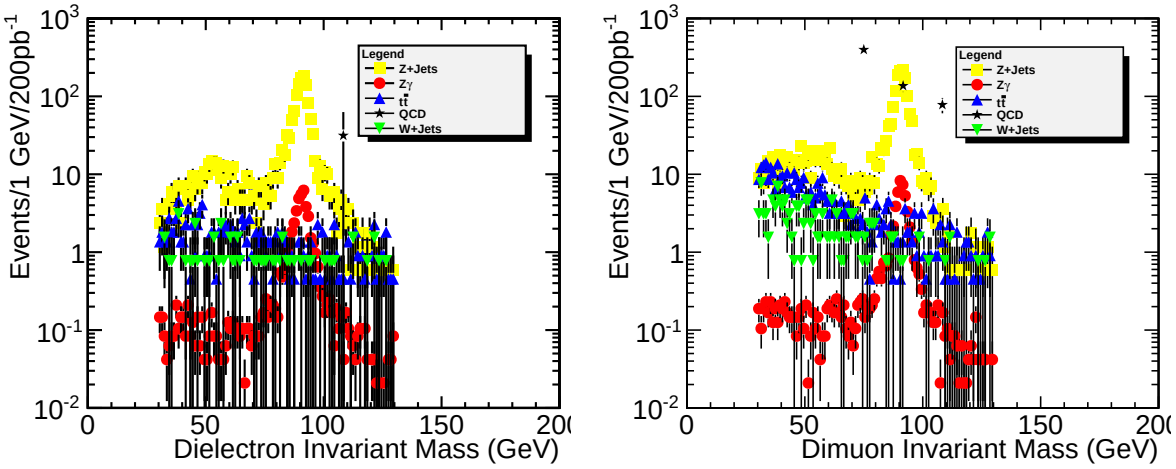

Figure 2: Dilepton mass distributions after preselection in electron and muon channels.

After preselection, we begin selecting the events by imposing lepton ID requirements. In the electron channel we use the version 1 tight electron ID, optimized for CMSSW 2.2.X, [11] and require that both electrons in the pair pass the ID. For the muon channel we require that both muons pass the "GlobalMuonPromptTight" ID [12]. Finally, for both lepton flavors we require that the relative combined isolation (Figure 3), $\frac{(ECAL+HCAL+Track)_{Isolation}}{pt_\ell}$, be less than .4.

The next set of selection cuts concern the kinematics of the dilepton, and dilepton + photon systems. We now constrain the dilepton mass (Figure 4) to 70 GeV $< M_{\ell\ell} <$ 100 GeV. This assymetric cut selects on-shell Z bosons and recovers events where the leptons from the Z have emitted bremsstrahlung. Then we apply a cut on the minimum ΔR between the leptons and each reconstructed photon in the event (Figure 5), requiring $min(\Delta R_{\ell\gamma}) > .7$. This removes photons from soft bremsstrahlung. Finally, we require that the invariant mass of the dilepton + photon system (Figure 6), $M_{\ell\ell\gamma}$, be greater than 98 GeV. This cut removes bremsstrahlung photons that were able to pass the previous ΔR cut. As seen in 4- 6, this set of cuts significantly reduces the amount of non-peaking background present in the set of events chosen at preselection.

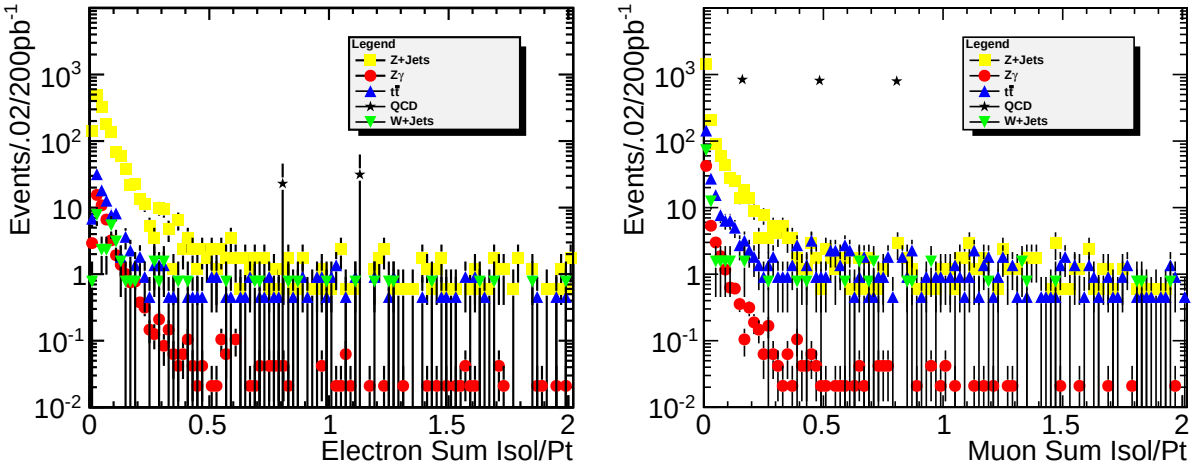

Figure 3: Relative lepton isolation in electron and muon channels.

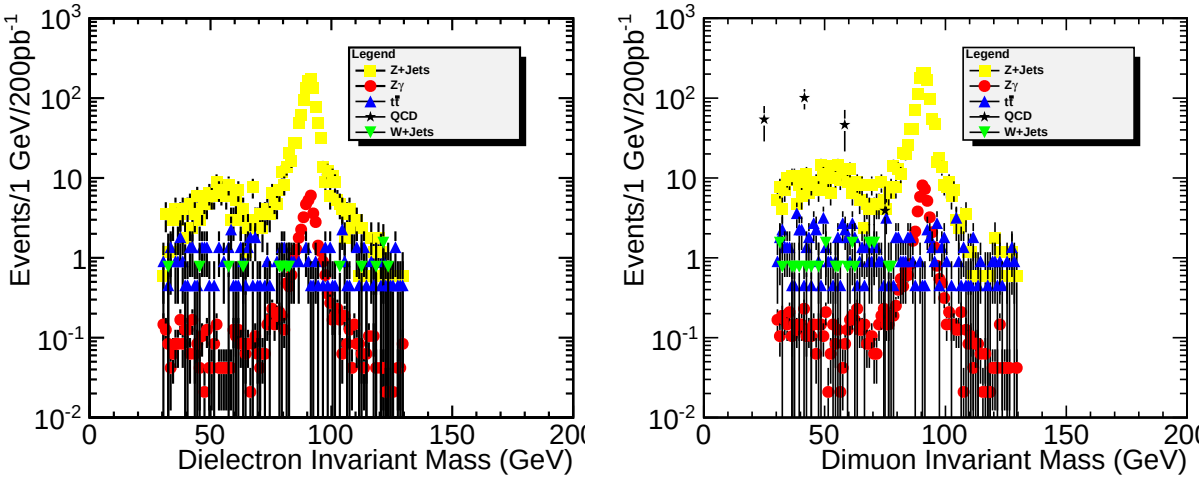

Figure 4: Dilepton invariant mass in electron and muon channels.

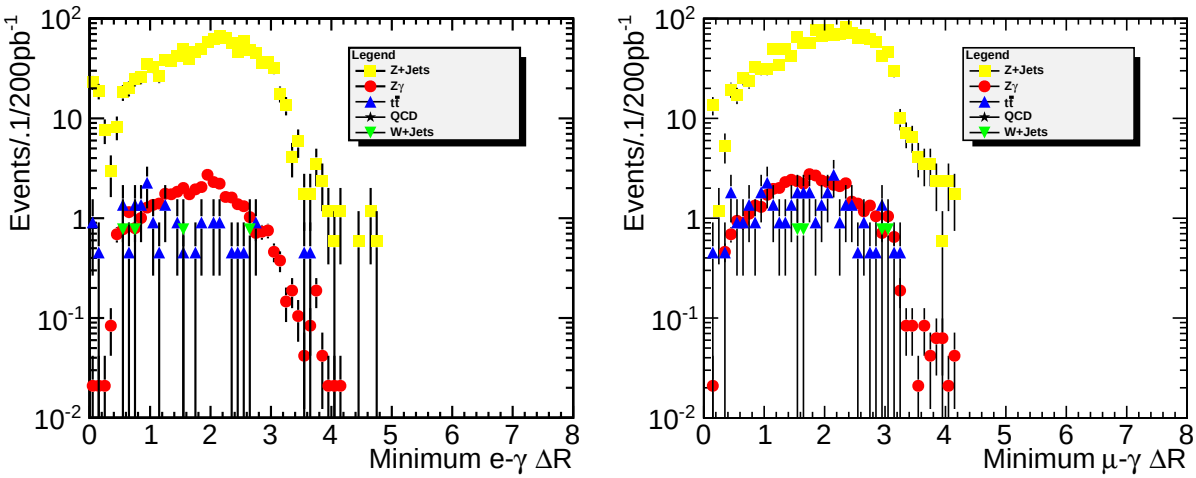

Figure 5: Minimum $\Delta R_{\ell\gamma}$ in electron and muon channels.

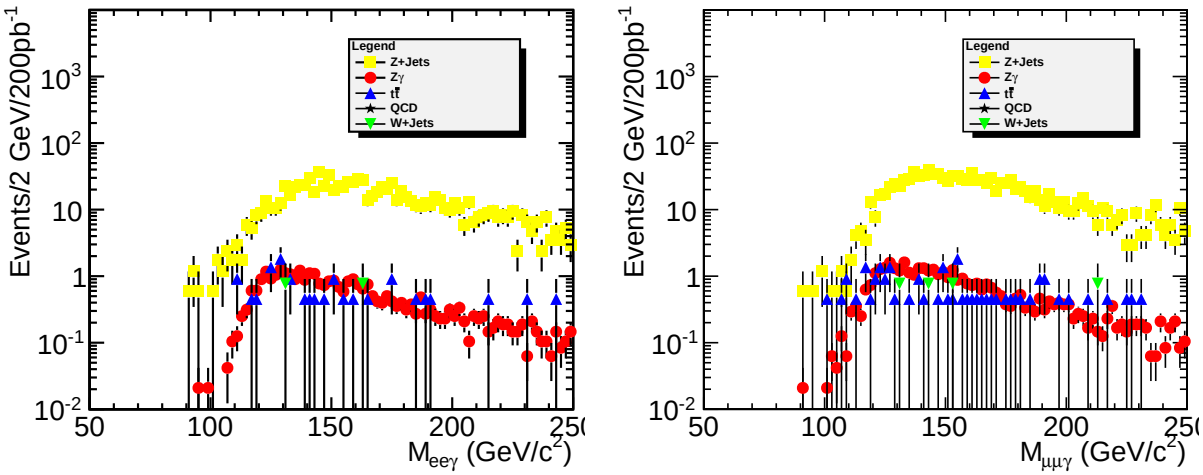

Figure 6: $M_{\ell\ell\gamma}$ in electron and muon channels.

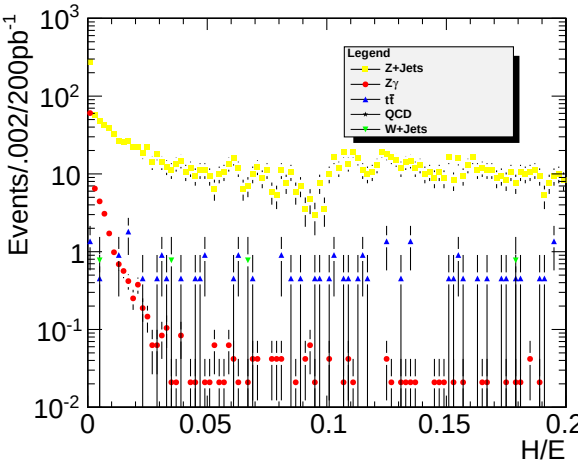

Figure 7: Reconstructed Photon H/E.

Next, we apply a set of cuts to identify real photons and reject fake photons. The first cut used to discriminate jets from photons is the ratio between activity in the HCAL and ECAL, or H/E. If a jet begins showering in the ECAL, the shower will typically deposit energy in the HCAL as well. A photon, instead, will deposit nearly all of its energy in the ECAL. Therefore, cutting tightly at H/E < 0.025 (Figure 7) accepts most of the signal while rejecting much of the $Z + Jets$ background.

Next we require that the number of tracks with $p_T > 0.3$ GeV in a cone centered on the supercluster centroid of $\Delta R < 0.4$ (Figure 8) be less than 3. This rejects the jet background and accepts both unconverted and converted photons since the jet can contain many charged particles.

The last photon ID cuts imposed are on ECAL, HCAL and Track isolation variables of the reconstructed photon (Figures 9, 10). The isolation sums are constructed by summing the energy in an annulus between a signal cone of 0.06 ΔR and an isolation cone of 0.4 ΔR, with both cones centered on the supercluster centroid. We require the ECAL isolation to be less than $7GeV + 0.0073 \cdot E_T^\gamma$, HCAL isolation to be less than $5GeV + 0.002 \cdot E_T^\gamma$ and Track Isolation less than $5GeV + 0.0073 \cdot E_T^\gamma$.

As shown in Table 2, QCD, $W + Jets$ and $t\bar{t}$ are trivial backgrounds since they require a sig-

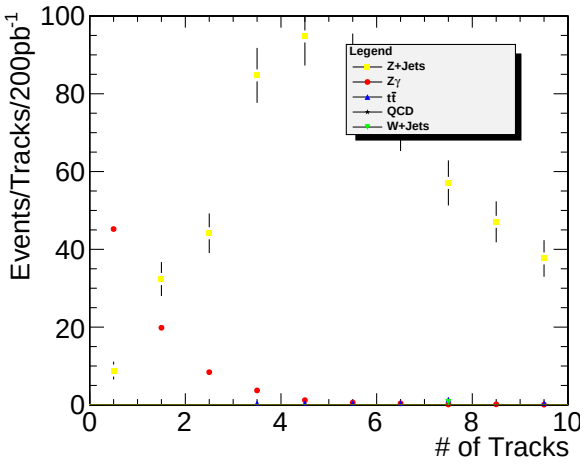

Figure 8: Number of reconstructed tracks within ΔR of 0.4 of the reconstructed photon.

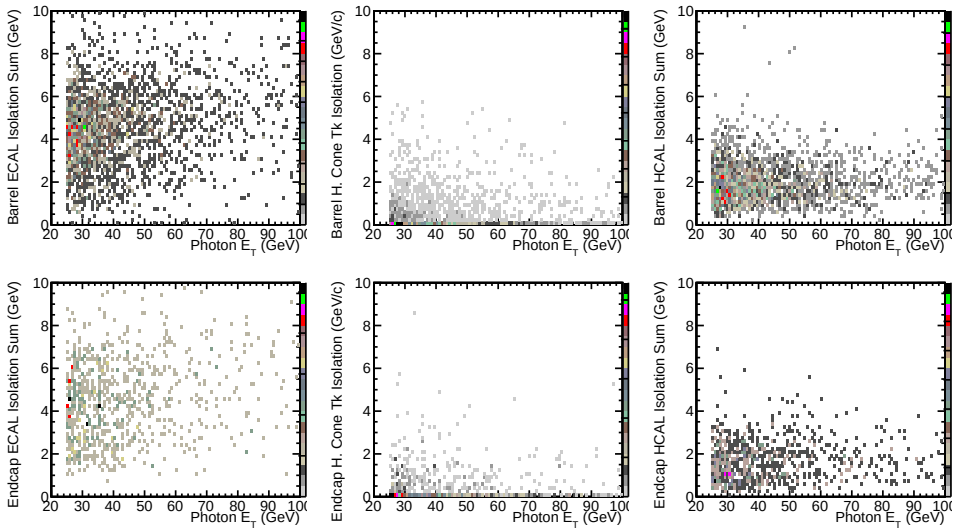

Figure 9: Photon isolation variables for signal in Barrel (top) and Endcaps (bottom).

nificant number of misreconstructions and are easily removed through kinematics cuts. The $Z + Jet$ events passing cuts are nearly all composed of Zs produced in association with jets that hadronize to π^0s.

The set of cuts used in this analysis effectively accepts the $Z\gamma$ signal while adequately rejecting background. The statistical errors given are calculated using gaussian statistics except where the number of events passing cuts is zero. In these instances, the error on zero is chosen arbitrarily to be one and is scaled by the weighting factor of the dataset. For $t\bar{t}$ the scale factor is roughly 0.5, for $W + Jets$ it is 0.8, and for QCD it is 5. The signal to background is 2.3$\pm$0.7 in the muon channel, and 3.1$\pm$1.1 in the electron channel. These are both in agreement with our rough theoretical guess of 3.

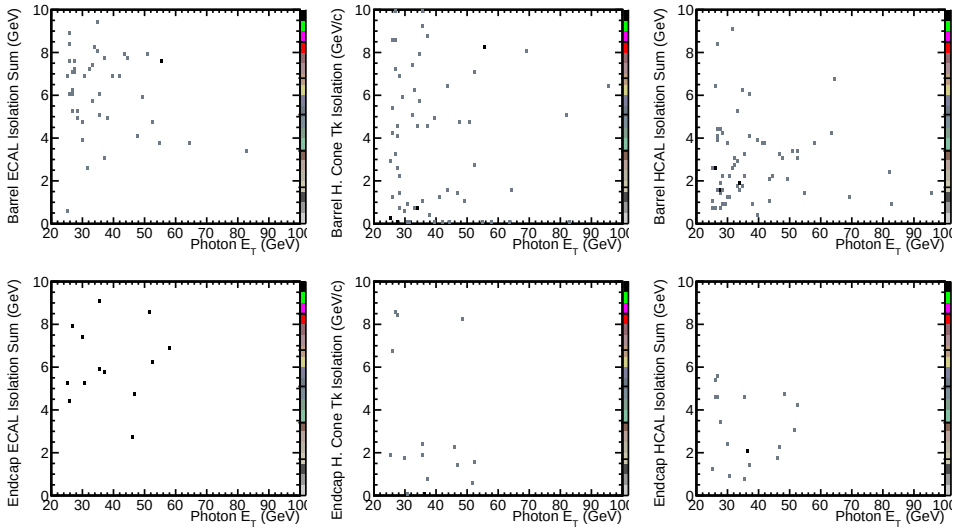

Figure 10: Photon isolation for background in Barrel (top) and Endcaps (bottom).

Table 2: List of cuts and their event yields; statistical errors are shown for final results.

Cut	$Z\gamma$	$Z + Jets$	$t\bar{t}$	$W + Jets$	Enriched QCD
Preselection	455	23k	8k	13k	3.8M
Acceptance and Lepton ID	106	3.8k	565	196	7.8k
Lepton Isolation	100	3.3k	187	29	200
70 GeV $< M_{\ell\ell} <$ 100 GeV	88	2.7k	54	6	0
$min(\Delta R_{\ell\gamma}) > .7$	82	2.5k	47	5	0
$M_{\ell\ell\gamma} >$ 98 GeV	82	2.5k	46	5	0
H/E $< .025$	80	646	5	1	0
$3 >$ Tracks in Solid Cone	73	85	0	0	0
Photon Isolation	68	26	0	0	0
Result in Muon Channel	37 ± 6.1	16.0 ± 4.0	$0\pm^{0.5}_{0.0}$	$0\pm^{0.6}_{0.0}$	$0\pm^{3.5}_{0}$
Result in Electron Channel	31 ± 5.5	10.0 ± 3.2	$0\pm^{0.5}_{0.0}$	$0\pm^{0.6}_{0.0}$	$0\pm^{3.5}_{0}$

2.3 Cut Efficiencies

In order to progress towards making a viable measurement of the $Z\gamma$ cross section at the LHC, the efficiencies for the identification and selection of various particles must be both well understood and flat. This ensures minimal bias from event selection, thus reducing the systematic error. The efficiencies for the electron and muon trigger and IDs are given in [13], [14], [11] and [12]. Photon reconstruction efficiency is analyzed in [15]. Therefore, we must analyze the efficiencies of the cuts used to select photons to complete the efficiency measurement. In this case we define the cut efficiency with the number of events after a cut divided by the number of events at preselection. The efficiency of each cut is plotted without the other photon ID cuts applied.

The H/E cut efficiency in the barrel and endcaps (Figure 11) is flat in the E_T and η of the photon, requiring that the photon be not near the ECAL crack region and has $E_T > 25GeV$. The structure in the η efficiency as the photon approaches the crack region and edge of the ECAL are caused by leakage of energy into the HCAL artifically increasing H/E for the photon. Since the H/E cut is tight compared to the standard photon ID cut of H/E < 0.2, this effect is more pronouced. To fix this in future studies, a H/E requirement that relaxes as detector edges are

approached would account for the leakage into the HCAL.

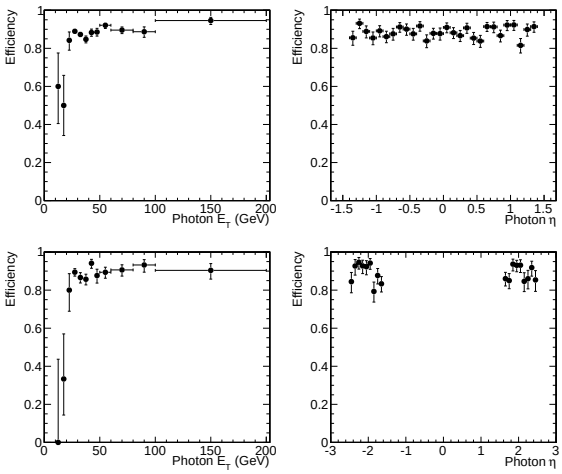

Figure 11: Signal efficiency for H/E $<$ .025 in Barrel (top) and Endcaps (bottom).

Requiring that the number of tracks in a hollow cone about the photon be less than 3 also results in flat efficiencies in photon η and E_T (Figure 12). This is expected since the cone defines a constant width in η, and any cut on the density of charged particles in equal sized $\Delta\eta$ regions should be roughly flat.

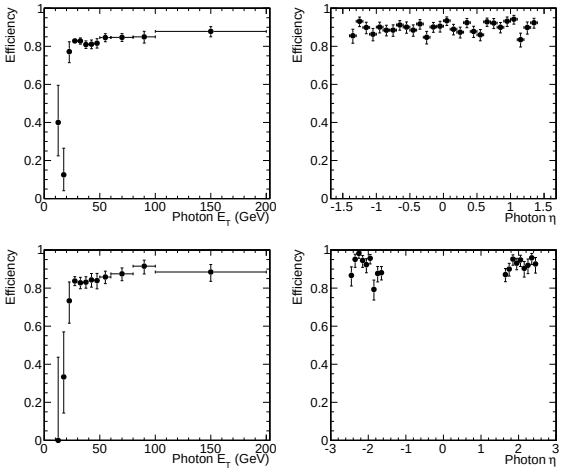

Figure 12: Signal efficiency for # Track $<$ 3 requirement in Barrel (top) and Endcaps (bottom).

Photon isolation sum requirements are the most powerful rejectors of the $Z + Jets$ background. The choice of relative vs. absolute isolation depends on the E_T range necessary for the analysis. Absolute isolation places cuts on the isolation sums directly, allowing the cuts to relax as a function of photon E_T. Since there is no scaling of the isolation sum, and hence no migration of low energy photons into the tails of the distribution, the efficiency remains flat for photon $E_T > 25GeV$ (Figure 13). Since this analysis requires good efficiency over a large range of photon E_T, we use absolute isolation requirements on ECAL, HCAL and Track isolation.

Relative isolation looks at the ratio of the photon's isolation sums to the photon's E_T, effectively relaxing the isolation requirement as photon E_T increases to account for leakage of the photon's energy into the isolation annulus. Using this type of isolation causes low energy photons to be

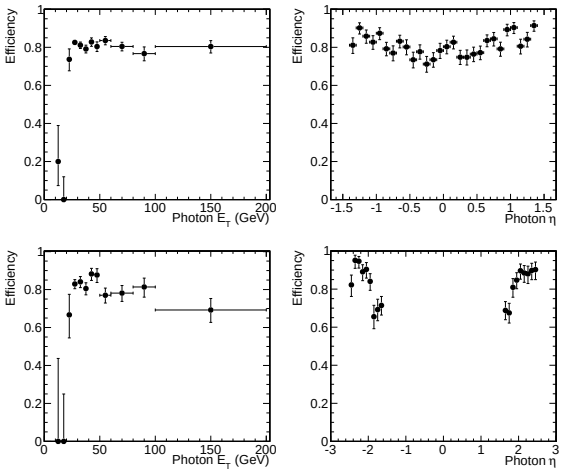

Figure 13: Photon isolation signal efficiency in Barrel (top) and Endcaps (bottom).

systematically pushed away from small values of the isolation variable, while improving the isolation of high energy photons. This effects the photon efficiency as a function of E_T resulting in a slow turn on curve (Figure 14) as the photon E_T becomes large enough to push the photon isolation below the cut threshold. For a high E_T analysis, as one would do for an anomalous coupling search, relative isolation becomes an acceptable cut variable.

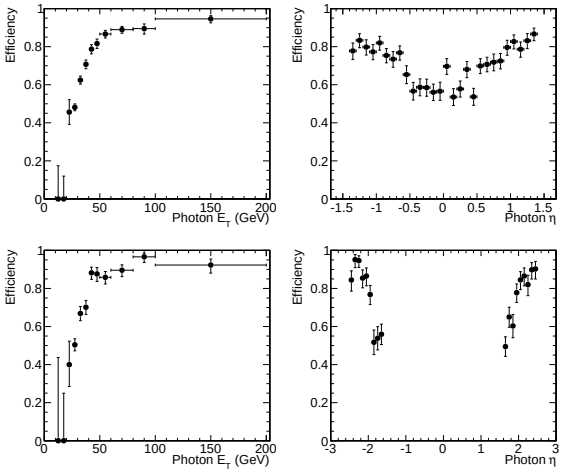

Figure 14: Photon relative isolation signal efficiency in Barrel (top) and Endcaps (bottom).

3 Analysis of $Z(\rightarrow ll)\gamma$ Using the Baur Generator

In order to produce events originating from processes beyond the Standard Model and, thus, be able to study the possibility of observing aTGCs in the $Z\gamma$ signal at CMS, an implementation of the Baur generator under the CMSSW framework was used [16]. We employ the Baur generator to produce signal events coming from both the SM and for a variety of values for the TGCs (§3.4). After a description of the interface of the generator to Pythia, this section presents the process of selecting SM signal against the main backgrounds, and concludes with a study of the sensitivity of CMS to the aTGCs in a model-independent way.

3.1 Baur generator - Pythia interface

As the "$Z\gamma$ Baur generator" produces weighted events, an unweighting technique should be used in order to pass them to Pythia for hadronization. The adopted technique is based on the determination of the maximum weight. For this, 10 million events were created and in order to stabilize the generator the first 0.5 million events have been skipped, then the maximum weight of the following 9.5 million events has been selected. This maximum weight is used to unweight the events, by comparing a random number with the ratio of each event's weight to the maximum; if the random number is smaller than the ratio, the event is selected and its weight is set to unit.
Another issue which arises after the unweighting of the events is that the Baur generator sums over all initial parton states, while Pythia should have a specific parton initial state. For this, the following technique was introduced in order to choose specific parton initial states for the selected unweighted events.
Using the 4-vectors of the initial state parton as input to the parton density function, the latter returns flavors distributed by their associated probabilities for the specific momentum slice. The initial state is selected randomly, taking into account the matrix element for $q\bar{q}$, qg, $\bar{q}g$. For each selected initial state all the possible flavour combinations that could originate from a pp collision are examined and the most probable one is selected.
Finally, in order to have a correct Baur generator - Pythia matching only the Born process of the Baur generator is activated.

3.2 Event selection within Standard Model

3.2.1 Muon selection

The SM signal sample was produced with the $Z\gamma$ Baur generator by setting the aTGCs of Eq.(1) to zero. The background samples used are *Z+Jets* and Inclusive Muon QCD from the official CSA08 production (Table 2, [10]); other backgrounds, i.e. $t\bar{t}$, WW, WZ, ZZ, turn out to be insignificant. All of the samples are analyzed under CMSSW 2.2.13 and the results are scaled to an integrated luminosity of $200pb^{-1}$. Note that the events are explicitly required to not contain initial state radiation, by vetoing non-Matrix Element ISR.
Both background and signal samples were produced in $\sqrt{s} = 10TeV$. The parton density function used with the Baur generator was `CTEQ Set 5L` since this leading-order parton density function is in common use in the CMS production. The following initial requirements were implemented in the production: For photons $P_t > 50GeV$, $|\eta| < 3$, and for leptons $P_t > 3GeV$, $|\eta| < 2.7$. We chose this high photon P_t since the presence of aTGCs is prominent at high photon P_t values. Finally, only the $ZZ\gamma$ vertex was generated.

We require all events to pass one of the High Level triggers HLT_Mu9 or HLT_DoubleMu3. These triggers use information from the Tracker and Muon system to select at least one (two)

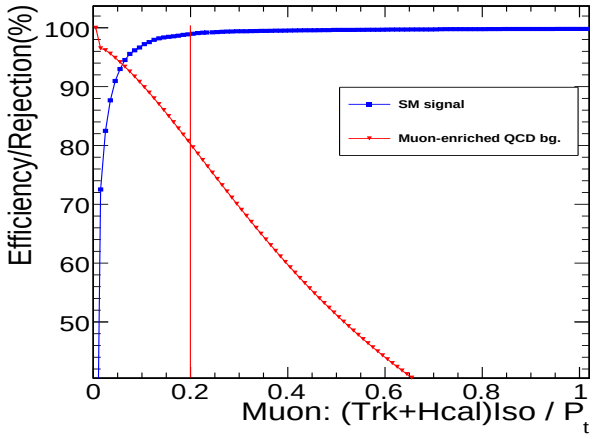

Figure 15: Selection efficiency (blue boxes) for signal muons (SM $Z\gamma$ sample with Baur generator) and rejection (red triangles) of Muon-enriched QCD background, as a function of the relative combined isolation from Tracker and HCAL (after muon identification cuts). A selection cut was set at 0.2, providing a signal efficiency of $\sim$ 99% and background rejection of $\sim$ 80%.

muon candidates with transverse momentum larger than $9 GeV/c$ ($3\,GeV/c$), with $d0 < 2cm$ [17]. For the preselection of muons, each candidate was required to fulfill general identification criteria quite similar to those of the identification scheme in [12], namely:

- have transverse momentum $p_T > 10\,GeV/c$,
- be in the region of pseudorapidity $|\eta| < 2.4$,
- have a silicon detector fit with $\chi^2/n.d.f. < 2$,
- originate from a vertex with $d0 \leq 0.2mm$ from the interaction point,
- leave more than 10 hits in the silicon detector.

Additionally, the relative combined isolation from Tracker and HCAL was used, with the sum of the deposition in a hollow cone of $0.01 < dR < 0.3$ around the particle for the Tracker and in a solid cone of $dR < 0.3$ for HCAL centered on the projection from the vertex. The relative isolation was required to be less than 0.2, ensuring high selection efficiency for the Zs ($\sim$ 99%), as tested against the Muon-enriched QCD background (rejection $\sim$ 80%) (Fig. 15).
Having identified the muons candidates, only events with exactly one pair of opposite-charge muons were accepted. After this criterion the Muon-enriched QCD background becomes insignificant.

The next step was the identification of bremsstrahlung radiation and the subsequent corrections on the muon pair. Bremsstrahlung photons were searched for among all reconstructed photons with H/E$<$ 0.2. The photons at a minimum distance from each muon were examined, and if that distance was $dR < 0.5$ the photon was accepted as bremsstrahlung radiation. From the matching at generated level (Fig. 16) it is obvious that this selection identifies the majority of the bremsstrahlung photons with $< 1\%$ contamination of $Z\gamma$ matrix element photons, and π^0's ($< 2\%$).

After applying the bremsstrahlung correction, the reconstructed mass of the muon pair was required to fall within a window of $10\,GeV/c^2$ around the Z pole mass. The invariant mass

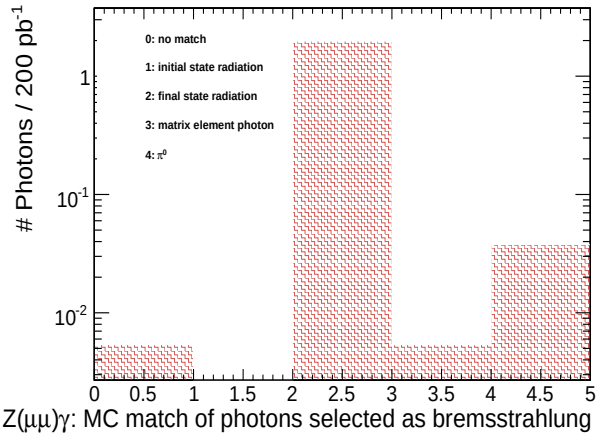

Figure 16: $Z(\rightarrow \mu^+\mu^-)\gamma$ channel: Matching at generated level for signal photons fulfilling the bremsstrahlung identification criteria.

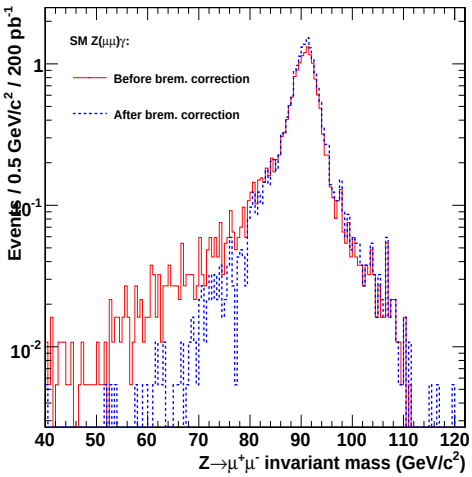

Figure 17: Dimuon invariant mass for signal events, before (solid line) and after applying bremsstrahlung correction (dashed).

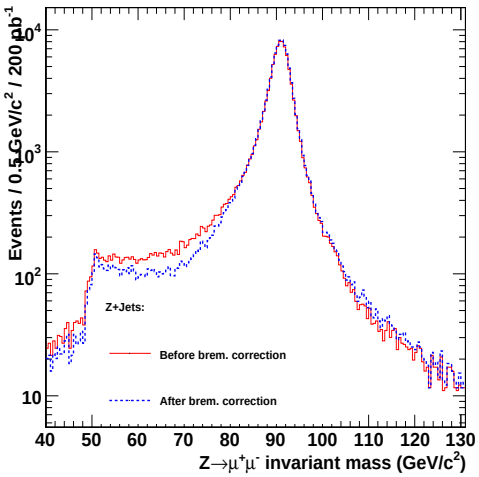

Figure 18: Dimuon invariant mass for $Z + Jets$ events, before (solid line) and after applying bremsstrahlung correction (dashed).

before and after the correction is plotted in Fig. 17 and Fig. 18 for $Z\gamma$ and $Z + Jets$ events respectively.

3.2.2 Electron selection

The analysis on the $Z(\rightarrow e^+e^-)\gamma$ channel starts by requiring the events not to contain initial state radiation, which was confirmed by matching with generator level information.
All of the analyzed events were required to pass the HLT_Ele15_LW_L1R trigger path. This trigger selects at least one electron candidate with transverse momentum larger than 15 GeV/c. For electron Pixel-matching windows, the large windows (LW, with very relaxed values) were used. The used trigger has a L1R (relaxed) seed type.[18]

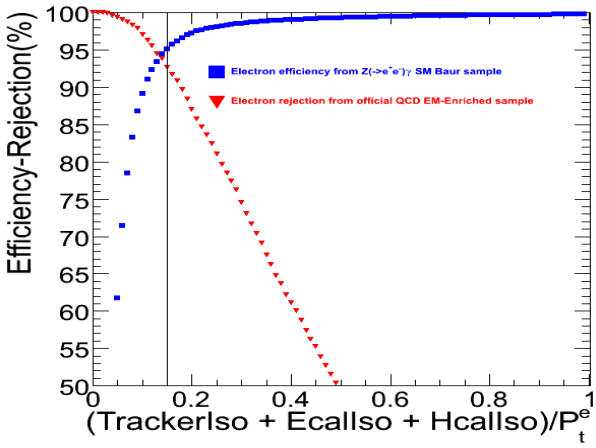

Figure 19: Selection efficiency (blue boxes) for signal electrons (SM $Z\gamma$ sample with Baur generator) and rejection (red triangles) of EM-enriched QCD background, as a function of the relative combined isolation from Tracker ECAL and HCAL (after electron identification cuts). A selection cut was set at 0.15, providing a signal efficiency of $\sim$ 95% and background rejection of $\sim$ 93%.

For the preselection of electrons each candidate was required to fulfill general identification criteria, namely:

- have transverse momentum $p_T > 20\,GeV/c$,
- be in the ECAL fiducial region($|\eta| < 2.5$ with ECAL Barrel - Endcap overlap region $1.442 < |\eta| < 1.556$ excluded),
- pass the "Tight" electron ID[19].

The relative combined isolation from Tracker, ECAL and HCAL was required to be less than 0.15, giving a $\sim$ 95% signal efficiency with $\sim$ 93% QCD EM enriched background rejection (Fig. 19). After selecting the electron candidates, only the events that had exactly one pair of opposite charge electrons were taken into account. This criterion makes the QCD EM enriched background insignificant.

At this point the $Z + Jets$ is the dominant background. In Fig. 20 we plot the invariant mass of the e^+e^- system for both Baur produced $Z(\rightarrow e^+e^-)\gamma$ and $Z + Jets$. Only events with reconstructed mass of the electron pair within a window of $10\,GeV/c^2$ around the Z pole mass are selected for further analysis.

3.2.3 Photon selection

In the last stage of event selection, we check the signal against the $Z + Jets$ background for photons in the final state. Candidates photon must fulfill some basic requirements:

- not be already characterized as bremsstrahlung photons, in $Z(\rightarrow \mu^+\mu^-)\gamma$ events,
- have transverse momentum $p_T > 60\,GeV/c$,
- lie in the ECAL fiducial region($|\eta| < 2.5$ with ECAL Barrel - Endcap overlap region $1.442 < |\eta| < 1.556$ excluded),
- leave no hits at the pixel detector,
- have a ratio of HCAL over ECAL activity H/E$<$ 0.2.

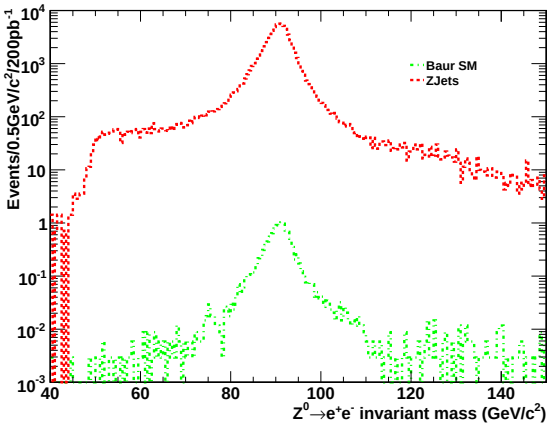

Figure 20: The reconstructed invariant mass for SM signal sample $Z(\rightarrow e^+e^-)\gamma$ and $Z + Jets$ background. Only events with reconstructed mass of the electron pair within a window of $10\,GeV/c^2$ around the nominal value of the Z mass were selected for further analysis.

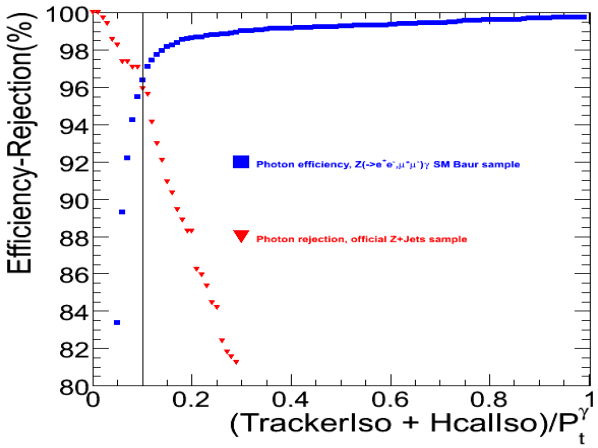

Figure 21: Selection efficiency (blue boxes) for the signal photons (both $Z((\rightarrow e^+e^-))\gamma$ and $Z(\rightarrow \mu^+\mu^-)\gamma$ channels) and and rejection (red trinagles) of the $Z + Jets$ background, as a function of the relative combined isolation from Tracker and HCAL in the Endcaps region (after photon identification cuts), for both $Z(\rightarrow \mu^+\mu^-)\gamma$ and $Z(\rightarrow e^+e^-)\gamma$ channels. A selection cut was set at 0.1.

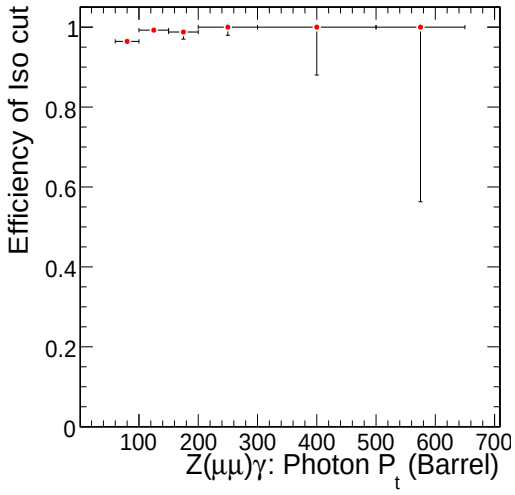

Figure 22: $Z(\rightarrow \mu^+\mu^-)\gamma$ channel:The relative combined isolation from Tracker and HCAL cut efficiency, for the signal photons as a function of their transverse momentum (ECAL Barrel).

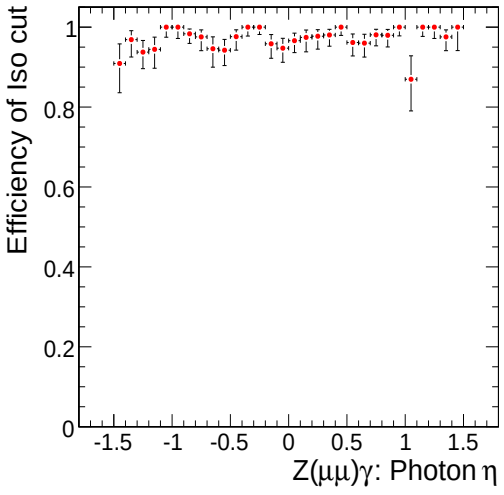

Figure 23: $Z(\rightarrow \mu^+\mu^-)\gamma$ channel:The relative combined isolation from Tracker and HCAL cut efficiency, for the signal photons as a function of their pseudorapidity (ECAL Barrel).

After these "basic cuts", the relative combined isolation from Tracker and HCAL eliminates strongly the background in both the ECAL barrel and, especially, the ECAL endcaps region. Therefore the relative combined isolation from the two detectors, which uses the deposition in a solid cone of $dR < 0.4$ with respect to the ECAL supercluster, was set to be less than 0.1. This choice retains in total $\sim 96\%$ of the signal events and rejects $\sim 96\%$ of the $Z + Jets$ background (Fig. 21).
In the case of muons the efficiency of this cut for the SM signal was found to be rather stable within 8.5% as a function of η, deteriorating only for $|\eta| > 2$ (Figs. 23, Fig. 25). In both Barrel and Endcaps regions the efficiency is almost stable and high ($> 95\%$) for final photons with $P_t > 60\,GeV$ (Figs. 22, Fig. 24).
Finally, a veto was set on events containing more than one photons which pass all of the above criteria.
After the selection process, almost all of the remaining $Z + Jets$ events contain π^0's misidentified as photons, with some contamination from final state radiation (Figs. 26, Figs. 27).

The event yields for the signal and the backgrounds after each step in the event selection process are summarized in Tables 3 and 4.

3.3 Anomalous TGCs

We investigate the sensitivity of CMS to aTGCs in the $Z\gamma$ channel in a way independent of a specific model, i.e. for continuous value ranges of the TGCs. For this, the transverse momentum distribution of the final photon was used in the likelihood fit, according to the method in [20].

The photon's transverse momentum (P_t^γ) is considered in general a strong discriminating vari-

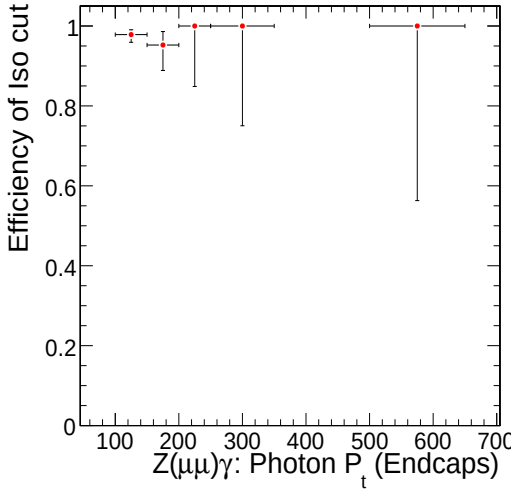

Figure 24: $Z(\rightarrow \mu^+\mu^-)\gamma$ channel:The relative combined isolation from Tracker and HCAL cut efficiency, for the signal photons as a function of their transverse momentum (ECAL Endcap).

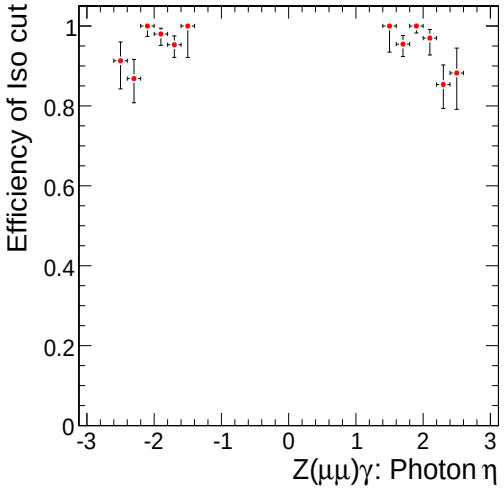

Figure 25: $Z(\rightarrow \mu^+\mu^-)\gamma$ channel:The relative combined isolation from Tracker and HCAL cut efficiency, for the signal photons as a function of their pseudorapidity (ECAL Endcap).

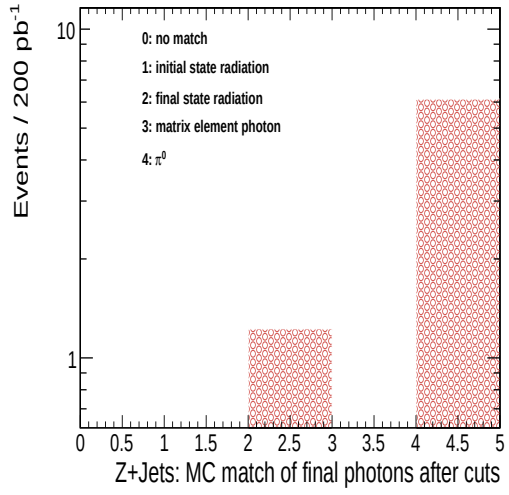

Figure 26: Matching at generated level for $Z + Jets$ background photons fulfilling the selection criteria of the $Z(\rightarrow \mu^+\mu^-)\gamma$ channel.

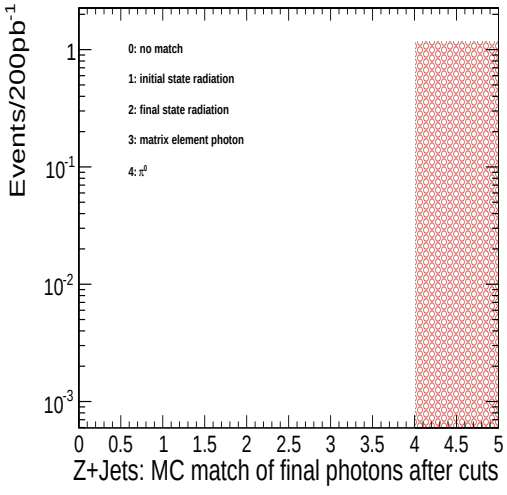

Figure 27: Matching at generated level for $Z + Jets$ background photons fulfilling the selection criteria of the $Z(\rightarrow e^+e^-)\gamma$ channel.

Table 3: $Z(\rightarrow \mu^+\mu^-)\gamma$ channel: List of cuts and their event yields for the study of aTGCs. (Normalized at $L = 200\,pb^{-1}$)

Cut	{00}	$Z + Jets$	Muon-enr.	{−−}	{−0}	{−+}	{0−}	{0+}	{+−}	{+0}	{++}
Initial	4751	$\sim 1.2 \cdot 10^6$	$\sim 1.2 \cdot 10^6$	9307	9297	9307	9333	9336	9210	9363	9400
No ISR	4453	$\sim 1.2 \cdot 10^6$	$\sim 1.1 \cdot 10^6$	8712	8693	8628	8725	8714	8568	8777	8811
Cross-sec.(pb)	0.12	3700	$\sim 509 \cdot 10^6$	0.144	0.188	0.383	0.186	0.186	0.363	0.188	0.144
Preselection	1	1	$\sim 2.4 \cdot 10^{-4}$	1	1	1	1	1	1	1	1
Efficiency											
Events at $L = 200pb^{-1}$	24	740,000	$\sim 24 \cdot 10^6$	29	38	73	37	37	73	38	29
HLT	23	173,084	$\sim 19 \cdot 10^6$	27	35	68	35	35	67	35	27
Muon Identif.	19	108,392	6385	23	29	56	27	28	55	30	23
and Isolation											
One Muon Pair	18	94,052	85	20	27	51	25	26	50	28	21
+ Mass Window											
Basic γ Identif.	10	218	0	12	18	39	17	17	38	19	13
γ Isolation	9.4 ± 3.1	7.4 ± 2.7	0	11.84 ± 3.4	17.4 ± 4.2	37.2 ± 6.1	16.0 ± 4.0	15.9 ± 4.0	36.6 ± 6.0	17.8 ± 4.2	12.0 ± 3.5

"+", "-" and "0" represent the values of the couplings h_3^Z, h_4^Z used in the production with the Baur generator, where $h_3^Z \in \{\pm 5 \cdot 10^{-2}, 0\}$, $h_4^Z \in \{\pm 1 \cdot 10^{-3}, 0\}$. "00" corresponds to the SM.

Table 4: $Z(\rightarrow e^+e^-)\gamma$ channel: List of cuts and their event yields for the study of aTGCs. (Normalized at $L = 200\,pb^{-1}$)

Cut	{00}	$Z + Jets$	EM-enr.	{−−}	{−0}	{−+}	{0−}	{0+}	{+−}	{+0}	{++}
Initial	9478	$\sim 1.2 \cdot 10^6$	$\sim 1.4 \cdot 10^6$	9483	9481	9475	9470	9478	9475	9471	9473
No ISR	8870	$\sim 1.2 \cdot 10^6$	$\sim 1.3 \cdot 10^6$	8841	8839	8730	8815	8829	8778	8839	8852
Cross-sec.(pb)	0.12	3700	$\sim 1 \cdot 10^8$	0.144	0.188	0.363	0.186	0.186	0.363	0.188	0.144
Preselection	1	1	1	1	1	1	1	1	1	1	1
Efficiency											
Events at $L = 200pb^{-1}$	24	740,000	$2 \cdot 10^{10}$	29	38	73	37	37	73	38	29
HLT	22	219,733	$\sim 4 \cdot 10^9$	26	34	66	33	33	66	34	26
Elec. Identif.	13	80,672	77,965	16	23	46	22	22	47	23	16
and Isolation,$\geq$2e											
One Elec. Pair	10	60,679	0	12	17	28	14	14	29	17	12
+ Mass Window											
Basic γ Identif.	5.5 ± 2.3	1.2 ± 1.1	0	6.9 ± 2.6	10.9 ± 3.3	20.3 ± 4.5	8.4 ± 2.9	8.4 ± 2.9	20.8 ± 4.6	11 ± 3.3	7.1 ± 2.7
+ γ Isolation											

"+", "-" and "0" represent the values of the couplings h_3^Z, h_4^Z used in the production with the Baur generator, where $h_3^Z \in \{\pm 5 \cdot 10^{-2}, 0\}$, $h_4^Z \in \{\pm 1 \cdot 10^{-3}, 0\}$. "00" corresponds to the SM.

able for processes beyond the Standard Model in the $Z\gamma$ signal [5]; for the set of aTGCs values used in this analysis, for P_t^γ above 200 GeV events beyond the SM dominate over the SM signal and background, while above 700 GeV the latter practically disappear (Figs. 28, 29). Another reason for using P_t^γ in the calculation of the sensitivity of CMS is the dependence of the amplitude of the process on it.

Suppose for simplicity that only two of the four anomalous couplings are non-zero, and in this study the CP-conserving h_3^Z and h_4^Z [Eq.(1)] were selected. Since the vertex amplitude is a linear function of the couplings, the cross section and the number of predicted events depend quadratically on them [6]. The number of events is, specifically, an elliptical paraboloidal function:

$$N(h_3^Z, h_4^Z) = N^{SM} + A \cdot h_3^Z + B \cdot h_4^Z + C \cdot {h_3^Z}^2 + D \cdot {h_4^Z}^2 + E \cdot h_3^Z \cdot h_4^Z \tag{2}$$

where N^{SM}: number of SM events, $A, ..., E$: coefficients.
This expression permits the prediction of the number of events for a range of values of the couplings when given only some of their combinations: Since for certain h_3^Z, h_4^Z the paraboloid becomes a function of the P_t^γs, if the events are binned according to their P_t^γ then a fit of the paraboloid to some simulated samples of different TGCs values suffices for the determination of the coefficients of Eq.(2) for each P_t^γ bin. In this way, it is possible to continue with predicting the number of events in a given P_t^γ bin for an arbitrary pair of h_3^Z, h_4^Z values.

This study uses nine samples which were produced with the combinations of the values $\{0, \pm 5 \cdot 10^{-2}\}$ for h_3^Z, and $\{0, \pm 1 \cdot 10^{-3}\}$ for h_4^Z, with a cut-off energy of $\Lambda = 2\,TeV$ and the minimum values for the dipole form factors exponent n (§1.1). As mentioned, the pair $(0, 0)$ corresponds to SM. The cuts discussed in §3.2, 3.3 were applied. We then fit the paraboloid over the number of events for the nine combinations in each P_t^γ bin (Figs. 30, 31) to obtain nine sets of the coefficients $A_i, ..., E_i$.

Next, the likelihood that P_t^γ distributions for anomalous TGCs, as obtained with the use of the paraboloids, are consistent with the expected SM data was calculated.
Half of the SM signal events produced with the Baur generator, along with the $Z + Jets$ background sample, were used as SM data. We assume the samples are Poisson-distributed, with the probability of measuring the number of events predicted by SM, N_i, when n_i^{ac} events are observed for a particular pair of couplings, being:

$$P_i = \frac{e^{-N_i} \cdot N_i^{n_i^{ac}}}{n_i^{ac}!}$$

Extended log-likelihood method was used, with the likelihood function $\mathcal{L}$ defined as the product of P_i over all P_t^γ bins (i), and its logarithm finally given by:

$$\ln \mathcal{L}(n^{ac}, h_3^Z, h_4^Z) = -n_{tot.}^{ac} + \sum_i N_i \cdot \ln n_i^{ac}$$

with each n_i^{ac} calculated of course with the corresponding paraboloid.

Finally, we determine the CMS sensitivity limits for h_3^Z, h_4^Z with $\Lambda = 2TeV$ to 95% confidence level (CL). We calculate the values with two-dimensional fits, with a confidence region corresponding to $\Delta \ln \mathcal{L}$ of 3 (Figs. 32, Figs. 33). We obtain separate limits for the h_3^Z, h_4^Z from the intersection of the ellipses with the axes. The separate limits occuring from the combined fit on both $Z(\rightarrow \mu^+\mu^-)\gamma$ and $Z(\rightarrow e^+e^-)\gamma$ samples (Fig. 34) are quoted and compared to existing

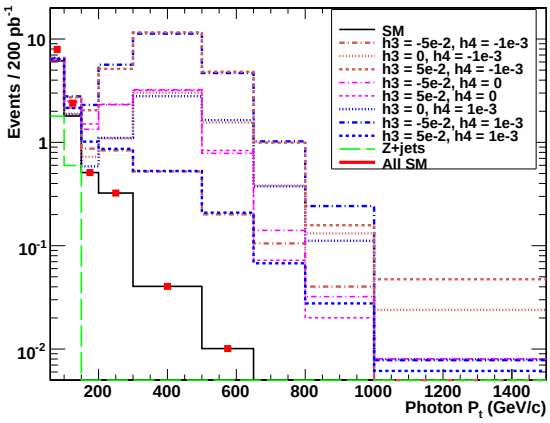

Figure 28: $Z(\rightarrow \mu^+\mu^-)\gamma$ channel: Photon transverse momentum for SM and anomalous TGCs (Baur generator).

data ([21]-[22]) in Table 5.

Table 5: Range of aTGCs values for experimental sensitivities at 95% CL, in combined $Z(\rightarrow \mu^+\mu^-)\gamma$ and $Z(\rightarrow e^+e^-)\gamma$ channels. For each quoted value, all other TGCs are assumed equal to zero.

	h_3^Z		h_4^Z	
LEP II	-0.20	0.07	-0.05	0.12
D0 ($1.1fb^{-1}$) [23]	-0.083	0.082	-0.0053	0.0054
CDF ($1.1fb^{-1}\,e, 2.0fb^{-1}\,\mu$)[22]	-0.083	0.083	-0.0047	0.0047
this study ($0.2fb^{-1}$)	-0.034	0.034	-0.00066	0.00069

(Tevatron results correspond to both $ZZ\gamma$ and $Z\gamma\gamma$ vertices, for $\Lambda = 1.2TeV$ and take into account next-to-leading order calculations. [21])

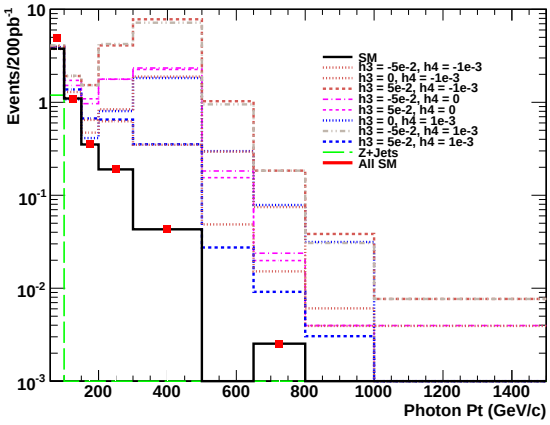

Figure 29: $Z(\rightarrow e^+e^-)\gamma$ channel: Photon transverse momentum for SM and anomalous TGCs (Baur generator).

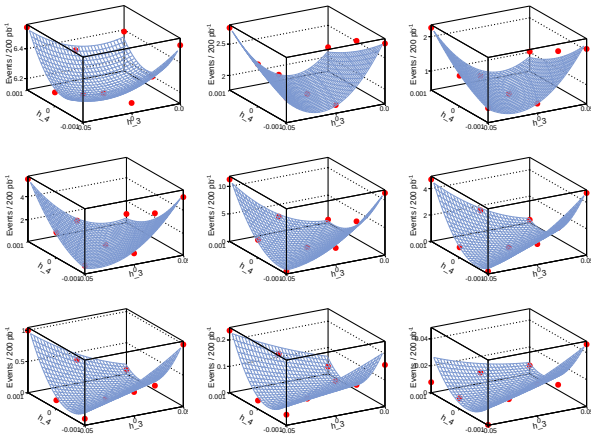

Figure 30: $Z(\rightarrow \mu^+\mu^-)\gamma$ channel: Fitting of Eq.(2) on the number of events for all pairs of TGCs values in each P_t^γ bin of Fig. 28.

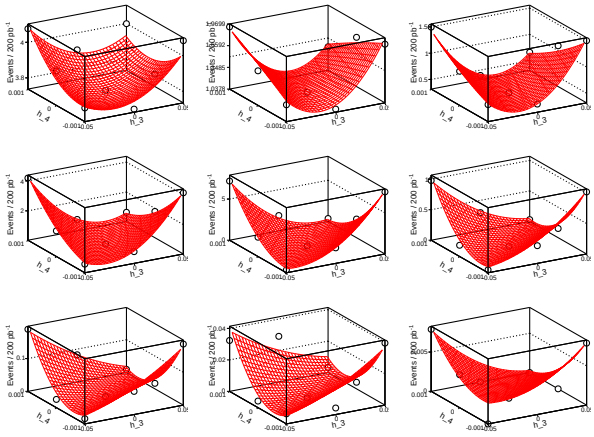

Figure 31: $Z(\rightarrow e^+e^-)\gamma$ channel: Fitting of Eq.(2) on the number of events for all pairs of TGCs values in each P_t^γ bin of Fig. 29.

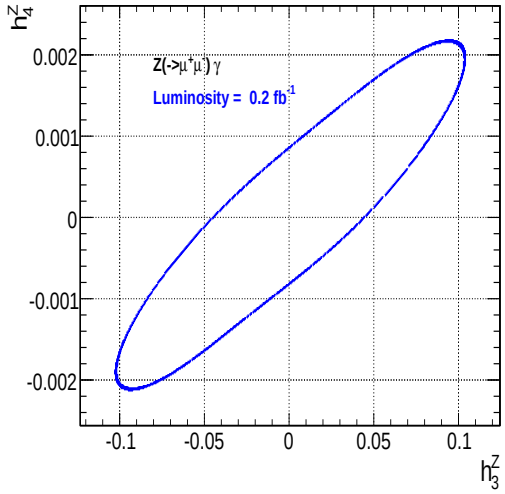

Figure 32: 95% CL contour in the h_3^Z, h_4^Z parameter space, in the $Z(\rightarrow \mu^+\mu^-)\gamma$ channel.

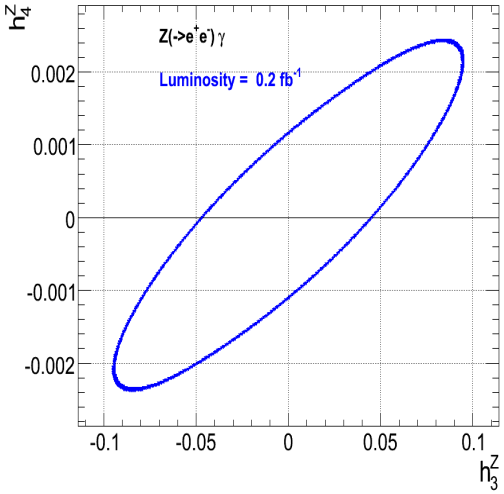

Figure 33: 95% CL contour in the h_3^Z, h_4^Z parameter space, in $Z(\rightarrow e^+e^-)\gamma$ channel.

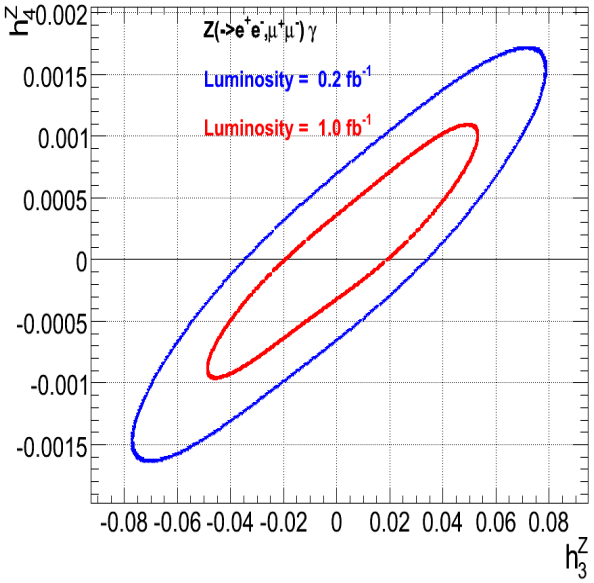

Figure 34: 95% CL contours in the h_3^Z, h_4^Z parameter space, in combined $Z(\rightarrow \mu^+\mu^-)\gamma$ and $Z(\rightarrow e^+e^-)\gamma$ channels.

4 Conclusion

In this paper we have outlined an initial plan for measuring the $pp \rightarrow Z(\rightarrow \ell^+\ell^-)\gamma$ event yields with CMS in the first $200pb^{-1}$. The pythia based analysis demonstrates resonable detector response to the $Z\gamma$ signal over a large range of photon E_T, and provides good statistics in the low photon E_T region, while rejecting most of the primary background. The aTGC muon and electron analyses show that, within the first $200pb^{-1}$ of data at 10 TeV, CMS can place new limits on the neutral $Z\gamma V$ triple gauge coupling, providing a versatile tool in the search for physics beyond the Standard Model. The analyses presented represent preliminary studies, and will be expanded to include full error analysis and general improvements from newer versions of CMSSW.

References

[1] K. Hagiwara, R. D. Peccei, D. Zeppenfeld, and K. Hikasa, "Probing the Weak Boson Sector in e+ e- → W+ W-," *Nucl. Phys.* **B282** (1987) 253. doi:10.1016/0550-3213(87)90685-7.

[2] F. M. Renard, "Tests of neutral gauge boson self-couplings with e+e—¿[gamma]Z," *Nuclear Physics B* **196** (1982), no. 1, 93 – 108. doi:10.1016/0550-3213(82)90304-2.

[3] J. Ellison and J. Wudka, "Study of Trilinear Gauge-Boson Couplings at the Tevatron Collider," *Annual Review of Nuclear and Particle Science* **48** (1998) 33–80, arXiv:hep-ph/9804322. doi:10.1146/annurev.nucl.48.1.33.

[4] A. Barroso, P. Nogueira, and J. C. Romao, "ELECTROMAGNETIC PROPERTIES OF THE Z BOSON. 2. WARD IDENTITIES FOR Z GAMMA GAMMA AND Z Z GAMMA GREEN'S FUNCTIONS," *Z. Phys.* **C33** (1986) 243–246. doi:10.1007/BF01411141.

[5] U. Baur and E. L. Berger, "Probing the weak-boson sector in $Z\gamma$ production at hadron colliders," *Phys. Rev. D* **47** (Jun, 1993) 4889–4904. doi:10.1103/PhysRevD.47.4889.

[6] U. Baur, T. Han, and J. Ohnemus, "QCD corrections and anomalous couplings in $Z\gamma$ production at hadron colliders," *Phys. Rev. D* **57** (Mar, 1998) 2823–2836. doi:10.1103/PhysRevD.57.2823.

[7] T. Sjostrand, S. Mrenna, and P. Skands, "PYTHIA 6.4 Physics and Manual," *JHEP* **05** (2006) 026, arXiv:hep-ph/0603175.

[8] D. Acosta, J. Adelman, T. Affolder, T. Akimoto, M. G. Albrow, D. Ambrose, S. Amerio, D. Amidei, A. Anastassov, K. Anikeev, A. Annovi, J. Antos, M. Aoki, G. Apollinari, T. Arisawa, J.-F. Arguin, A. Artikov, W. Ashmanskas, A. Attal, F. Azfar, P. Azzi-Bacchetta, N. Bacchetta, H. Bachacou, W. Badgett, A. Barbaro-Galtieri, G. J. Barker, and V. E. Barnes, "Measurement of $W\gamma$ and $Z\gamma$ Production in $p\bar{p}$ Collisions at $s = 1.96TeV$," *Phys. Rev. Lett.* **94** (Feb, 2005) 041803. doi:10.1103/PhysRevLett.94.041803.

[9] K. Grogg, C. Lazaridis, S. Dasu, J. Efron, P. Klabbers, W. Smith, L. Kaur, S. Beri, and B. Dahmes, "A Study of W/Z+Jet Events Using Electron Modes," **CMS Analysis Note in Preparation**.

[10] "Summer08: Full Simulation SM Production for Physics at 10 TeV," *https://twiki.cern.ch/twiki/bin/view/CMS/ProductionSummer2008*.

[11] F. Beaudette, C. Charlot, E. Delmeire, C. Rovelli, and Y. Sirois, "Search for a Light Standard Model Higgs Boson in the $H \to WW^* \to e^+\nu e^-\bar{\nu}$ Channel," **CMS NOTE 2006/114**.

[12] M. Mulders, I. Bloch, E. James, A. Everett, D. Barge, C. Campagnari, P. Kalavase, V. Krutelov, D. Kovalskyi, J. Ribnik, and N. Amapane, "Muon Identification in CMS," **CMS AN-2008/98**.

[13] H. Yoo, A. Everett, L. Chang, and N. Neumeister, "Level-3 Muon Trigger Performance on CRAFT data," **CMS AN 2009/127**.

[14] F. Agostino and M. Pieri, "HLT Selection of Electrons and Photons," **CMS NOTE 2006/078**.

[15] S. Ganjour, L. Millischer, S. Ahuja, S. Chauhan, B. Choudhary, C. Kuo, Y. Lu, S. Yu, R. Lu, T. Orimoto, V. Chetluru, V. O'Dell, V. Gaultney, S. Linn, Y. Kim, Y. Lee, A. Debenedetti, T. Kolberg, N. Marinelli, and M. Anderson, "Towards a Measurement of the Isolated Photon Cross Section at CMS," **CMS Analysis Note in Preparation**.

[16] K. Karafasoulis and A. Kyriakis, "Integration of Baur Zgamma MC Generator into CMSSW framework," *https://twiki.cern.ch/twiki/bin/view/CMS/BaurZgamInterface*.

[17] "HLT paths for the 8E29 "core" menu," *https://twiki.cern.ch/twiki/bin/view/CMS/TSG_18_II_09_8E29*.

[18] "Egamma HLT in CMSSW," *https://twiki.cern.ch/twiki/bin/view/CMS/SWGuideEgammaHLT*.

[19] "Cut Based Electron ID," *https://twiki.cern.ch/twiki/bin/view/CMS/SWGuideCutBasedElectronID*.

[20] T. Müller, D. Neuberger, and W. Thümmell, "Sensitivities for anomalous WW and ZZ couplings at CMS," **CMS AN-2000/17**.

[21] A. Lyon, "Testing the Standard Model with Wgamma and Zgamma at the Tevatron,". doi:0810.3766v1.

[22] "Zgamma Limits on Neutral Anomalous Couplings in ppbar Collisions at sqrt(s)=1.96TeV," *http://www-cdf.fnal.gov/physics/ewk/2009/zgamma/ZgammaWebPage/index.html*.

[23] D. Collaboration", "Zgamma Production and Limits on Anomalous ZZgamma and Zgammagamma Couplings in ppbar Collisions at sqrt(s)=1.96TeV," *Phys. Lett. B* **653** (2007) 378. doi:0705.1550v2.